arXiv:1610.03169v1 [cond-mat.mes-hall] 11 Oct 2016

Dimensional reduction of the Luttinger Hamiltonian and g-factors of holes in symmetric two-dimensional semiconductor heterostructures

D. S. Miserev, O. P. Sushkov[1]

[1]*School of Physics, University of New South Wales, Sydney, Australia*

(Dated: October 12, 2016)

The spin-orbit interaction of holes in zinc-blende semiconductors is much stronger than that of electrons. This makes the hole systems very attractive for possible spintronics applications. In three dimensions (3D) dynamics of holes is described by well known Luttinger Hamiltonian. However, most of recent spintronics applications are related to two dimensional heterostructures where dynamics in one direction is frozen due to quantum confinement. The confinement results in dimensional reduction of the Luttinger Hamiltonian, 3D→2D. Due to interplay of the spin-orbit interaction, the external magnetic field, and the lateral gate potential imposed on the heterostructure the reduction is highly nontrivial and not known. In the present work we perform the reduction and hence derive the general effective Hamiltonian which describes spintronics effects in symmetric two-dimensional (2D) heterostructures. In particular, we do the following, (i) derive the spin-orbit interaction and the Darwin interaction related to the lateral gate potential, (ii) determine the momentum dependent out-of-plane g-factor, (iii) point out that there are two independent in-plane g-factors, (iv) determine momentum dependencies of the in-plane g-factors.

PACS numbers: 71.70.Ej, 73.22.Dj, 71.18.+y

I. INTRODUCTION

Spin orbit interaction (SOI) in cubic zinc-blende semiconductors is of topical interest because of various spintronics applications and devises. It is well understood that SO interaction is very different for the conduction band (electrons) and for the valence band (holes). Electrons in the conduction band originate from atomic s-orbitals and therefore they have spin 1/2. There are two SOI for electrons, the Dresselhaus interaction[1] which is due to inversion asymmetry in bulk and Rashba interaction[2] which is usually due to asymmetric 2D interfaces. The SO interactions are relatively week in semiconductors with light atoms like GaAs, and they can become significant in semiconductors with heavy atoms like InAs and InSb[3,4].

The valence band (holes) originates from atomic $p_{3/2}$ orbitals, therefore the effective spin is $S = 3/2$, and hence the SOI quadratic in spin is possible. This SOI is always strong, even in Si it is comparable with kinetic energy. In this sense holes in zinc-blende semiconductors are always 'ultrarelativistic', the SOI is comparable or even larger than kinetic energy. The quadratic in spin SOI is described by Luttinger Hamiltonian[5]. Of course, the standard Dresselhaus interaction[1] and even an additional Dresselhaus-like interaction[6] exist for holes too. They are relatively week in semiconductors with light atoms like GaAs, and they become more important in semiconductors with heavy atoms like InAs and InSb[7,8]. Nevertheless, the most important spin-orbital physics comes from the Luttinger Hamiltonian, and this is what we consider in the present work.

Most, if not all, modern hole-based spintronics devises are essentially two-dimensional (2D). This includes quantum point contacts (QPC)[9–15], quantum dots[16–19], as well as heterostructures used in Subnikov-de Haas measurements[8,20–23]. These systems are based on quantum wells. The well freezes dynamics in one direction due to quantum confinement. The confinement results in dimensional reduction of the Luttinger Hamiltonian, 3D→2D, only the in-plane coordinate and associated in-plane momentum $\boldsymbol{k}$ remain as dynamic variables. Due to interplay of the spin-orbit interaction, the external magnetic field, and the lateral gate potential imposed on the heterostructure spin dynamics of the arising 2D system is highly nontrivial. For example, for out-of-plane magnetic field the g-factor of hole is significantly modified by the virtual 3D dynamics[24–27]. The virtual 3D dynamics is even more important for response to the in-plane magnetic field[13,28]. Effects of magnetic field in some dimensionally reduced systems have been considered previously, but only in some limiting cases[13,24–29]. The spin-orbital effects related to the lateral gate potential to the best of our knowledge have been considered before only in a very special limit related to the artificial graphene[30]. In the present work we consider the most general situation with respect to both the magnetic field and the lateral gate potential. This analysis is applicable to QPCs, quantum dots, and for laterally modulated superlattices.

In the present work we derive the general two-dimensional effective Hamiltonian resulting from the dimensional reduction of the Luttinger Hamiltonian in a symmetric heterostructure. We develop a general method for the dimensional reduction valid for any symmetric heterostructure. To be specific we present results of numerical calculations for two different types of heterostructure, (i) parabolic quantum well, (ii) infinite rectangular quantum well in GaAs and InAs. In the present work we do not consider asymmetric heterostructures which necessarily generate the Rashba-type effective interaction. Such heterostructures require techniques beyond that developed in the present work. Therefore, the asymmetric

case will be a subject of a separate work.

The paper is organized as follows; in Section II we briefly remind the very well-known calculation of hole sub-bands, see e.g Ref.[7] We use results of this section in the rest of the paper. In Section III we introduce the effective Hamiltonian as Ginzburg-Landau-type gradient expansion over lateral potential. Section IV addresses momentum dependent in-plane g-factors. In Section V we derive the spin-orbit interaction related to the lateral potential. To do so we use the scattering amplitude method first developed for Breit interaction in quantum electrodynamics[31]. Usage of the method allows us to find also the Darwin term in the effective Hamiltonian. Section VI addresses momentum dependent out-of-plane g-factor which is the most technically involved part. Finally, we present our conclusions in Section VII.

II. SUB-BANDS

We start this section from reminding the very well known description of 2D sub-bands which we use in subsequent sections. Non-interacting holes in bulk conventional semiconductors are described by the Luttinger Hamiltonian[5]. In this paper, we consider so-called spherical approximation to the Hamiltonian

$$H_L = \left(\gamma_1 + \frac{5}{2}\overline{\gamma}_2\right)\frac{\mathbf{p}^2}{2m} - \frac{\overline{\gamma}_2}{m}\left(\mathbf{p}\cdot\mathbf{S}\right)^2 \ , \tag{1}$$

where[32]:

$$\overline{\gamma}_2 = \frac{2\gamma_2 + 3\gamma_3}{5} \ .$$

Here $\mathbf{p}$ is 3D quasi-momentum; $\mathbf{S}$ is the spin $S = 3/2$; γ_1, γ_2, and γ_3 are Luttinger parameters; and m is the free electron mass. It is known that there is also a non-spherical part of the Luttinger Hamiltonian

$$\delta H_L = p_i p_j S_m S_n T^{(4)}_{ijmn} \ , \tag{2}$$

where the irreducible 4th rank tensor $T^{(4)}_{ijmn}$ depends on the orientation of the cubic lattice. The tensor is proportional to $\gamma_2 - \gamma_3$. Since in the large spin-orbit splitting materials $\gamma_2 \approx \gamma_3$ the rotationally noninvariant part of the Hamiltonian is small and we neglect it. Of course, there are some effects that are essentially related to the rotational asymmetry[8,20,33,34] and in this cases (2) cannot be neglected. The general techniques developed in the present work can accommodate the rotational anisotropy. Nevertheless, for clarity of presentation we omit the anisotropy in the present paper.

Impose the quantum well potential $W(z)$ on the system, the Hamiltonian reads

$$H = H_L + W(z) \ . \tag{3}$$

The well confines dynamics along z-axis leading to 2D sub-bands $\varepsilon_{n,\boldsymbol{k}}$, where $\boldsymbol{k} = (k_x, k_y) = (p_x, p_y)$ is the 2D momentum, and integer n enumerates the bands. To be specific, we present herein numerical results for parabolic and infinite rectangular quantum wells in GaAs and InAs, see Fig.1.

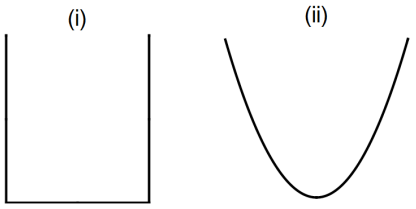

FIG. 1: Shape of quantum well: (i) infinite rectangular, (ii) parabolic.

$$\begin{aligned} (i) \ : \quad & W(z) = \begin{cases} 0, & z \in (-d/2, d/2) \\ \infty, & \text{otherwise.} \end{cases} \\ (ii) \ : \quad & W(z) = \frac{m\omega_z^2 z^2}{2} \end{aligned} \tag{4}$$

Since z-confinement is very strong, the most important part of (3) comes from terms proportional to p_z^2,

$$\begin{aligned} H_0 \ &= \ \left(\gamma_1 + \frac{5}{2}\overline{\gamma}_2 - 2\overline{\gamma}_2 S_z^2\right)\frac{p_z^2}{2m} + W(z) \\ &+ \ \left(\gamma_1 - \frac{5}{4}\overline{\gamma}_2 + \overline{\gamma}_2 S_z^2\right)\frac{k^2}{2m} \ . \end{aligned} \tag{5}$$

Note that the simple in-plane kinetic energy $\propto k^2/2m$ is also included in H_0. It is evident from (5) that the lowest energy sub-band comes from $S_z = \pm 3/2$. It is usually called the first "heavy hole" subband (HH1). There is also HH2 sub-band, etc. The sub-bands with $S_z = \pm 1/2$ are called "light hole" sub-bands, LH1, LH2, etc. The Hamiltonian (3) can be represented as

$$\begin{aligned} & H = H_0 + V \\ & V = -\frac{\overline{\gamma}_2}{4m}\left[k_+^2 S_-^2 + k_-^2 S_+^2 + \right. \\ & \left. + \{p_z, k_+\}\{S_z, S_-\} + \{p_z, k_-\}\{S_z, S_+\}\right] \ . \end{aligned} \tag{6}$$

Here $\{...\}$ denotes the anticommutator. Evaluation and diagonalization of the Hamiltonian matrix of (6) in the basis of eigenstates of (5) is straightforward. The sub-bands arising from this diagonalization for GaAs and InAs are plotted in Fig.2 for both quantum wells considered here.

Luttinger paramters used in the calculations are presented in Table I. Let us introduce the momentum unit for parabolic and rectangular wells:

$$k_0 = \begin{cases} 0.5\sqrt{m\omega_z} & \text{parabolic} \\ 2.0/d & \text{rectangular} \end{cases} \tag{7}$$

It is useful to note that for rectangular quantum well with $d = 20$ nm, the momentum $k = k_0$ corresponds to

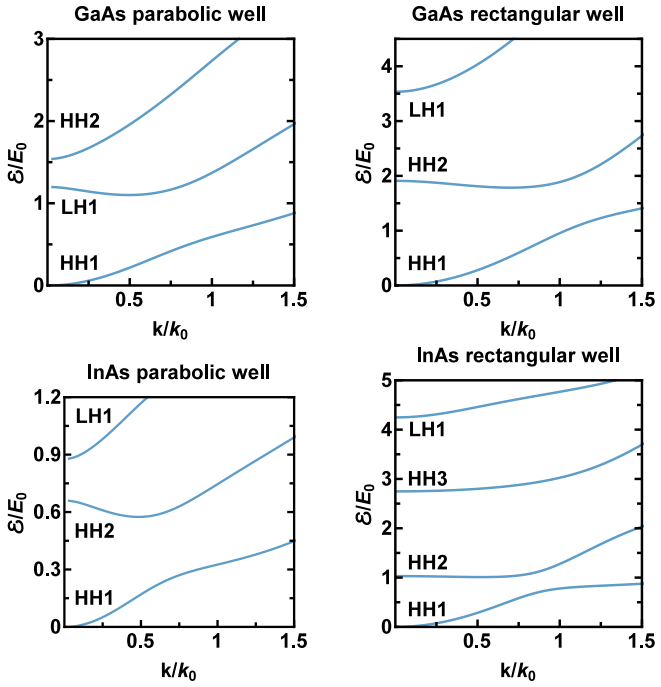

FIG. 2: Hole sub-bands for parabolic quantum well and for infinite rectangular well in GaAs and InAs. Momentum is given in units of k_0, see Eq.(7), and energy in units of E_0, see Eq.(8).

	γ_1	γ_2	γ_3	$\overline{\gamma}_2$	κ
GaAs	6.85	2.1	2.9	2.58	1.2
InAs	20.4	8.3	9.1	8.78	7.6

TABLE I: Luttinger parameters for GaAs, and InAs.

the hole density $1.6 \times 10^{11} cm^{-2}$, this is about a typical experimental density. Energies we express in units

$$E_0 = \frac{\gamma_1 k_0^2}{2m}. \tag{8}$$

The energy scale for rectangular quantum well of the width $d = 20$ nm is $E_0 = 2.6$ meV which corresponds to experimental values of the Fermi energy. Effective mass $m^* = k\left(\frac{d\varepsilon}{dk}\right)^{-1}$ increases with the in-plane momentum due to non-parabolic corrections, see Fig. 3.

Let us impose now a magnetic field B and a lateral potential $U(x, y)$ on the heterostructure. The magnetic field manifests itself in the long derivatives in the Hamiltonian (5), (6), $\boldsymbol{p} \to \boldsymbol{p} - e\boldsymbol{A}$, and in the Zeeman term $-2\kappa\mu_B(\boldsymbol{B}\cdot\boldsymbol{S})$. Here, $\boldsymbol{A}$ is the vector potential, e is the elementary charge, μ_B is the Bohr magneton. Values of the material specific parameter κ are listed in the Table I, see e.g. Ref.[7] Thus, the total 3D Hamiltonian reads

$$\begin{aligned} H &= H_0(\boldsymbol{\pi}) + V(\boldsymbol{\pi}) - 2\kappa\mu_B(\boldsymbol{B}\cdot\boldsymbol{S}) + U(x,y) \\ \boldsymbol{\pi} &= \boldsymbol{p} - e\boldsymbol{A} \end{aligned} \tag{9}$$

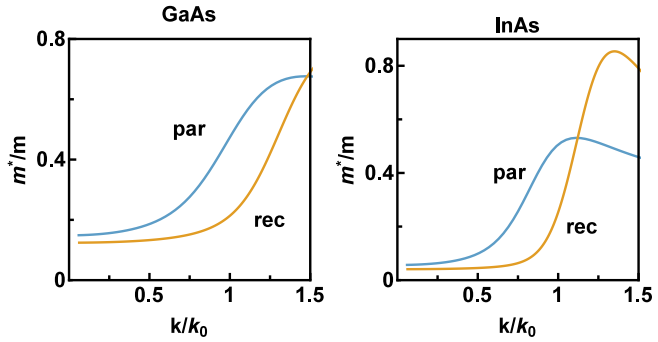

FIG. 3: The effective mass in the HH1 subband. Parabolic and rectangular quantum wells in GaAs and InAs.

III. EFFECTIVE 2D HAMILTONIAN, GRADIENT EXPANSION

We consider here only HH1 sub-bands, see Fig. 2. This implies that the Fermi energy is below the bottom of the first excited sub-band. The HH1 subband is double degenerate due to the Kramers theorem. The standard way to describe the Kramers doublet is to introduce the effective spin $s = 1/2$ (pseudo-spin) with related Pauli matrixes $\boldsymbol{\sigma}$. The correspondence at $k = 0$ is very simple, $|\uparrow\rangle = |S_z = 3/2\rangle$, $|\downarrow\rangle = |S_z = -3/2\rangle$.

The effective 2D Hamiltonian can depend only on 2D variables, it cannot contain z and p_z. We assume that the gate lateral potential is smooth, $k\nabla U \ll U$, so we can use the gradient expansion of the potential. As soon as we understand this point, the kinematic form of the Hamiltonian is unambiguously dictated by symmetries and gauge invariance:

$$\begin{aligned} H_{2D} &= \varepsilon(\boldsymbol{\pi}) + U(x,y) \\ &+ \{\alpha(\boldsymbol{\pi}), (\boldsymbol{s}\cdot[\boldsymbol{\nabla}U\times\boldsymbol{\pi}])\} + \frac{1}{2}\{\beta(\boldsymbol{\pi}), \Delta U\} \\ &- g_{zz}(\boldsymbol{\pi})\mu_B B_z s_z \\ &- \frac{\mu_B}{2}\overline{g}_1(\boldsymbol{\pi})(B_+\pi_+^2 s_- + B_-\pi_-^2 s_+) \\ &- \frac{\mu_B}{2}\overline{g}_2(\boldsymbol{\pi})(B_-\pi_+^4 s_- + B_+\pi_-^4 s_+). \end{aligned} \tag{10}$$

Here, $\mathbf{s} = \boldsymbol{\sigma}/2$ is pseudo-spin; $B_\pm$, $\pi_\pm$, and $s_\pm$ are defined in the standard way, $B_\pm = B_x \pm iB_y$ etc, $\{\ldots\}$ is anti-commutator. We stress again that all the variables, gradients, etc. in the Hamiltonian are two dimensional. While the dispersion $\varepsilon(k)$ has been discussed in the previous section, the functions $\alpha(k)$, $\beta(k)$, $g_{zz}(k)$, $\overline{g}_1(k)$, and $\overline{g}_2(k)$ will be determined in subsequent sections. Like the dispersion they are isotropic, i.e. depend on $k = |\boldsymbol{k}|$. It is useful to underline the most important points concerning Eq. (10). (i) This is a gradient expansion up to the second gradient of U, we neglect third derivatives of the gate potential. The Darwin term, $\propto \Delta U$, is spin independent and therefore not very interesting. We keep it only for completeness, since like in Dirac equation it comes together with the usual spin-orbit and the coefficients α

and β have the same dimension. (ii) Due to the gauge invariance, all the coefficients, α, β, g_{zz}, $\overline{g}_1$, and $\overline{g}_2$ depend on the kinematic momentum $\boldsymbol{\pi} = \boldsymbol{k} - e\boldsymbol{A}$, $\boldsymbol{A}$ depends only on x and y. (iii) The α- and β-terms contain anticommutators. (iv) We neglect powers of magnetic field higher than two in the spin response, for example, we neglect the kinematic structures like $B_+^3\sigma_-$. However, it is very easy to restore these terms with the developed technique. (v) The angular momentum selection rule for the effective spin σ_- is $\Delta S_z = -3$. Therefore, there are two generally independent in-plane g-factors, the functions $\overline{g}_1$ and $\overline{g}_2$. (vi) The Hamiltonian must be symmetric over all rotations around z-axis and π-rotations around x-axis. Therefore, $\overline{g}_1$ and $\overline{g}_2$ are real. Of course, α, β and g_{zz} are real too.

Now we proceed to the calculation of functions which enter the effective Hamiltonian (10), we start from the in-plane g-factors.

IV. IN-PLANE G-FACTORS

There are two independent in-plane g-functions, $\overline{g}_1(k)$ and $\overline{g}_2(k)$, see Eq. (10). In order to find these functions, we numerically diagonalize the Luttinger Hamiltonian (9) with $U = 0$ and with magnetic field directed along x-axis, $\boldsymbol{B} = (B, 0, 0)$. We use the vector potential in the following gauge:

$$\mathbf{A} = (0, -Bz, 0). \tag{11}$$

In this gauge, the in-plane momentum $\boldsymbol{k}$ is a good quantum number, $\psi \propto e^{ik_x x + ik_y y}$. Therefore $\boldsymbol{k}$ enters (9) as a simple number, so only the one-dimensional z-confinement problem needs to be diagonalized numerically. We calculate the magnetic spin-splitting of HH1 sub-band at different values of $\boldsymbol{k}$. As we have to find two different functions, we perform calculation twice with $\boldsymbol{k} = (k, 0)$ and with $\boldsymbol{k} = (0, k)$. Effective momentum dependent g-factors

$$\begin{aligned} g_1 &= k^2\overline{g}_1(k) \\ g_2 &= k^4\overline{g}_2(k) \end{aligned} \tag{12}$$

for GaAs and InAs and for parabololic and rectangular quantum wells are plotted in Fig.4.

At small k, the g-factors (12) scale as high powers of momentum. Therefore, it is instructive to plot also $\overline{g}_1$ and $\overline{g}_2$. These functions have dimensions $[1/k^2]$ and $[1/k^4]$ respectively. We use powers of k_0, Eq.(7), to balance the momentum dimension. Plots of $k_0^2\overline{g}_1(k)$ and $k_0^4\overline{g}_2(k)$ are presented in Fig.5. Zero momentum value of $\overline{g}_1$ can be calculated analytically with usual perturbation

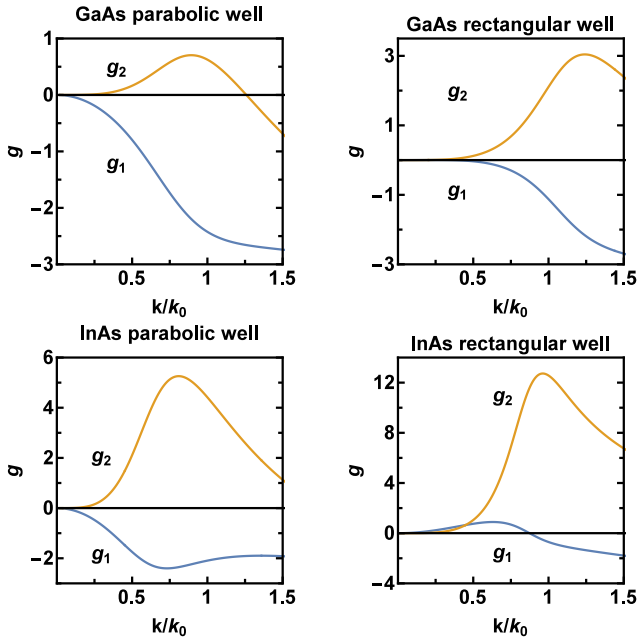

FIG. 4: Effective in-plane HH1 g-factors, see Eq.(12), versus momentum. The g-factors are presented for parabolic and rectangular confinement in GaAs and InAs.

theory, the result reads

$$\overline{g}_1(0) = -3\overline{\gamma}\left(\kappa Z_1 - 4\overline{\gamma}Z_2 - \overline{\gamma}Z_3 + 2\kappa\overline{\gamma}Z_4\right) \tag{13}$$

$$Z_1 = -2\sum_{n=1}^{\infty}\frac{|\langle 1H|nL\rangle|^2}{m(\varepsilon_{nL} - \varepsilon_{1H})}$$

$$Z_2 = 2i\sum_{n=1}^{\infty}\frac{\langle 1H|z|nL\rangle\langle nL|p_z|1H\rangle}{m(\varepsilon_{nL} - \varepsilon_{1H})}$$

$$Z_3 = -2i\sum_{n=1}^{\infty}\frac{\langle 1H|\{z, p_z\}|nL\rangle\langle nL|1H\rangle}{m(\varepsilon_{nL} - \varepsilon_{1H})}$$

$$Z_4 = 2\sum_{n=1}^{\infty}\frac{|\langle 1H|p_z|nL\rangle|^2}{m^2(\varepsilon_{nL} - \varepsilon_{1H})^2}\ .$$

The zero momentum value of $\overline{g}_1$ has been calculated in Ref.[13] with only Z_1 and Z_2 terms taken into account. Z_4 and, especially, Z_3-term are important, this is why our values of $\overline{g}_1(0)$ differ from that of Ref.[13] shown in Fig.5 by red dots on the vertical axis.

The most important conclusion of this section is that at $k \approx 1$ where most experiments are performed, both invariant g-factors g_1 and g_2 are equally important, see Fig. 4.

V. SPIN-ORBIT INTERACTION DUE TO THE LATERAL GATE POTENTIAL

To calculate the spin-orbit interaction and the Darwin term in the effective Hamiltonian (10) we employ the scattering amplitude method which is usu-

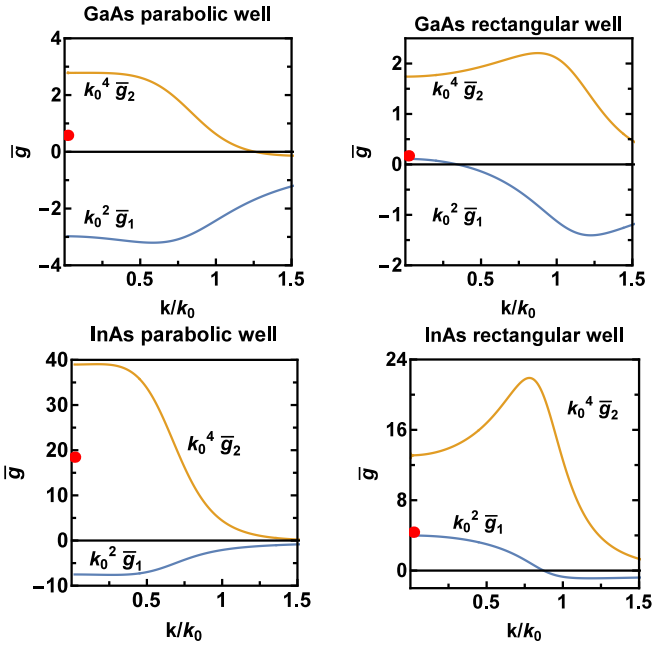

FIG. 5: Functions $\overline{g}_1(k)$ and $\overline{g}_2(k)$ related to the in-plane g-factors, see Eq. (12). The functions are presented for parabolic and rectangular quantum wells in GaAs and InAs. To balance dimension, we plot the functions multiplied by a corresponding power of k_0. Red points on the vertical axes indicate values of $\overline{g}_1(k=0)$ calculated using equations in Ref.[13] The points must be compared with our blue lines.

ally used for derivation of Breit interaction in quantum electrodynamics[31]. This is a technically efficient way to proceed from a full multicomponent description to the effective two-component wave function. Magnetic field is not relevant to this problem, so in this section the magnetic field is zero. Consider scattering of a hole from a weak lateral potential limited in space, for example, from a Gaussian potential,

$$U(x,y) = U_0 e^{-(x^2+y^2)/a^2} \ . \tag{14}$$

Actual shape of the potential is not important, the only important point is that the potential is weak and limited in space, so the scattering problem makes sense. The idea of the method is to calculate the Born scattering amplitude, $\boldsymbol{k} \to \boldsymbol{k}'$. The scattering amplitude calculated with the effective Hamiltonian (10) must be the same as the amplitude calculated with 3D Hamiltonian (9). This allows one to find functions $\alpha(k)$ and $\beta(k)$ in (10).

An eigenstate of the Hamiltonian (5), $|S_z, n, \boldsymbol{k}\rangle$, possess a definite value of the in-plane momentum $\boldsymbol{k}$ and a definite value of $S_z = -3/2, -1/2, 1/2, 3/2$,

$$|S_z, n, \boldsymbol{k}\rangle = e^{i\boldsymbol{k}\cdot\boldsymbol{r}} |S_z, n\rangle \ . \tag{15}$$

Here, the index n enumerates transverse modes (z-standing waves). The diagonalization of the Hamiltonian (6) which is described in the section II results in energy bands and in wave functions expressed in terms of (15).

In particular, the wave function of the $|\uparrow, \boldsymbol{k}\rangle$ state of the HH1 band is of the form

$$|\uparrow, \boldsymbol{k}\rangle = \sum_{S_z} \sum_{n} a_n(S_z, k) k_+^{(3/2-S_z)} |S_z, n, \boldsymbol{k}\rangle \ , \tag{16}$$

where the momentum dependent coefficients $a_n(S_z, k)$ are determined by the numerical diagonalization, and the phase factor, $k_+^{(3/2-S_z)}$ is dictated by the conservation of total angular momentum. The Born scattering amplitude is given by the matrix element of the scattering potential U between the initial and final states,

$$f_{\mathbf{k}'\mathbf{k}} = \langle\uparrow, \boldsymbol{k}'|U(\mathbf{r})|\uparrow, \boldsymbol{k}\rangle = U_{\mathbf{q}} \sum_{l=0}^{3} b_l(k) \cdot (k'_- k_+)^l \ , \tag{17}$$

where

$$b_l(k) = \sum_{n=1}^{\infty} \left| a_n(\frac{3}{2} - l, k) \right|^2 \ , \tag{18}$$

$U_{\boldsymbol{q}}$ is the Fourier transform of $U(\mathbf{r})$, and $\boldsymbol{q} = \mathbf{k}' - \mathbf{k}$ is the momentum transfer. When calculating (17) using (16), we take into account that $\mathbf{k}'^2 = \mathbf{k}^2$ due to the energy conservation. Note that the wave function normalization condition reads

$$1 = b_0 + k^2 b_1 + k^4 b_2 + k^6 b_3 \ . \tag{19}$$

The product $k'_- k_+$ which enter Eq. (17) reads

$$k'_- k_+ = k^2 - \frac{1}{2} q^2 + i[q_x k_y - q_y k_x] \ . \tag{20}$$

The first power of the square bracket in this equation is responsible for the skew scattering. Therefore, comparing the $[\boldsymbol{q} \times \boldsymbol{k}]$ term from (17) with the scattering amplitude calculated with the α-term in Eq. (10) we find the following expression for α

$$\alpha(k) = b_1(k) + 2k^2 b_2(k) + 3k^4 b_3(k) \ . \tag{21}$$

Similarly, the terms proportional to q^2 in (17) contribute to the Darwin term. Comparing the q^2 term from (17) with the scattering amplitude calculated with the β-term in Eq. (10) we find the following expression for β

$$\beta(k) = \frac{1}{2} b_1(k) + 2k^2 b_2(k) + \frac{9}{2} k^4 b_3(k) \ . \tag{22}$$

There are also higher powers of q in Eq. (17), up to q^6, they correspond to higher gradients in the gradient expansion of the effective Hamiltonian. We neglect the higher gradients in (10) assuming that U is sufficiently smooth. However, in principle, the scattering amplitude method Eq. (17) allows to find all the terms of the gradient expansion.

Since the numerical diagonalization described in section II gives all coefficients of the HH1 wave function, it is easy to calculate α and β using Eqs. (18),(21),(22). Functions $\alpha(k)$ and $\beta(k)$ for parabolic and rectangular quantum wells in GaAs and InAs are plotted in Fig. 6. Both α and β have dimension $[1/k^2]$. To balance the dimension in Fig. 6, we plot $k_0^2\alpha$ and $k_0^2\beta$.

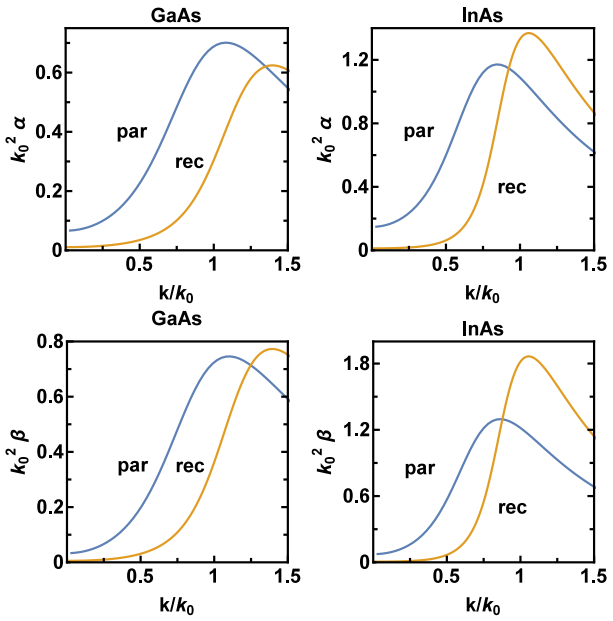

FIG. 6: The spin-orbit α and the Darwin β functions for the lateral gate potential, see Eq. (10). The functions are presented for parabolic and rectangular quantum wells in GaAs and InAs and multiplied by powers of k_0 to make them dimensionless.

VI. OUT-OF-PLANE G-FACTOR

A naive value of g_{zz} is $g_{zz} = 6\kappa$, see Eq. (9) and Ref.[7] Virtual orbital 3D dynamics strongly influences this value. The effect of the virtual dynamics at k=0 has been calculated previously, it leads to a very significant reduction of the g-factor[24–27]

$$g_{zz}(0) = 6\kappa - 12\overline{\gamma}^2 \sum_{n=1}^{\infty} \frac{|\langle 1H|p_z|nL\rangle|^2}{m(\varepsilon_{nL} - \varepsilon_{1H})} \ , \qquad (23)$$

The g-factor is significantly different from the naive value. For example, the g-factor in GaAs where $6\kappa = 7.2$, is $g_{zz}(0) = 7.2 - 5.15 = 2.05$ for parabolic quantum well and $g_{zz}(0) = 7.2 - 2.6 = 4.6$ for rectangular quantum well. Our goal in this section is to calculate the entire function $g_{zz}(k)$ defined in Eq. (10). One possibility is to calculate Landau levels with the Hamiltonian (9) and then look at the spin splitting of the levels. This approach used in Ref.[27] for the rectangular well indicated a significant dependence of g-factor on Landau level. However, this method is rather technically involved and computationally expensive. Here we use a different method, we destroy Landau levels by a gate potential and calculate linear spin response.

Let us consider the parabolic gate potential,

$$U(x) = \frac{m\omega_x^2 x^2}{2} \ , \qquad (24)$$

which restricts the hole propagation in the x-direction. The vector potential for the out-of-plane magnetic filed $\boldsymbol{B} = (0, 0, B)$ is taken in the following gauge:

$$\mathbf{A} = (0, B \cdot x, 0) \ . \qquad (25)$$

So, the y-component of momentum is conserved and we set $k_y = 0$. In this situation, the long momentum that enters the full Luttinger Hamiltonian (9) is $\boldsymbol{\pi} = (p_x, -eBx, p_z)$. Since there is no dynamics along the y-direction, $e^{ik_y y} = 1$, effectively the Hamiltonian (9) becomes two-dimensional, only the x- and the z-directions are nontrivial. A brute force numerical diagonalization of this Hamiltonian is straightforward. We consider energy below the bottom of the first excited band, see Fig. 2, so all quantum states we consider originate from the lowest HH1 band. Due to the gate confinement (24), the spectrum is discrete, it is described by an integer quantum number $n_x = 1, 2, 3...$, and due to the magnetic field, the Kramers degeneracy of each n_x level is lifted as it is illustrated in Fig. 7. For numerical calculations with (9),(24)

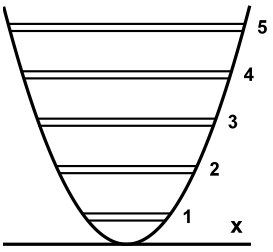

FIG. 7: Magnetic field split oscillator levels with $n_x = 1, 2, 3, ...$ in the parabolic gate potential (24).

we use sufficiently small values of ω_x, $\omega_x \sim 0.01$, so that there are about 100-150 oscillator levels within the energy span of the HH1 band. It is worth noting that the spectrum is not equidistant because the dispersion $\varepsilon(p)$ is not parabolic. Magnetic field which we consider in this analysis is even smaller than ω_x, $B \ll \omega_x$. In practice, we first diagonalize (9),(24) numerically at $B = 0$, and then we account for the weak magnetic field by usual perturbation theory. As result, we find the Zeeman splitting of each oscillator level, see Fig. 7,

$$\Delta\varepsilon = -g(\varepsilon)\frac{1}{2}\mu_B B\sigma_z \ . \qquad (26)$$

Here, ε is energy corresponding to the oscillator level with quantum number n_x. The outcome of the brute force numerical calculation is the function $g(\varepsilon)$.

The next question is: how to deduce the function $g_{zz}(k)$ in Eq.(10) from $g(\varepsilon)$ obtained in the numerical calculation described in the previous paragraph? To answer this question, let us articulate the problem in terms of the effective 2D Hamiltonian (10). With gate potential (24) the effective Hamiltonian takes the following form

$$H_{2D} = \varepsilon(k_x) + \frac{m\omega_x^2}{2}(x^2 + 2\beta) - [g_{zz} + 2m^2\omega_x^2\{\alpha, x^2\}]\frac{1}{2}\mu_B B\sigma_z \ . \qquad (27)$$

Actually, the Hamiltonian becomes 1D. We remind that $\alpha(k_x)$ is the coefficient in the gate spin orbit interaction and $\beta(k_x)$ is the coefficient in the gate Darwin term, both functions have been determined in section V. The α-term in (27) is due to $\pi_y = -eBx$. Eq. (27) is written in linear in B approximation, we neglect $\pi_y^2 = (eBx)^2$ which is quadratic in B. There is an important point to note about the Hamiltonian (27): the Zeeman splitting arises not only due to g_{zz}, there is a part of the splitting which is due to the gate potential. This point is important for understanding of experiments with quantum point contacts and quantum dots in an out-of-plane magnetic field.

Let us set B=0 in Eq.(27),

$$H_{2D}^{(0)} = \varepsilon(k_x) + \frac{m\omega_x^2}{2}(x^2 + 2\beta) \ . \tag{28}$$

In semiclassical limit, $n_x \gg 1$, Eq. (28) determines x^2 as function of k_x at a given energy ε.

$$x^2 = \frac{2}{m\omega_x^2}[\varepsilon - \overline{\varepsilon}(k_x)]$$
$$\overline{\varepsilon}(k_x) = \varepsilon(k_x) + m\omega_x^2\beta(k_x) \ . \tag{29}$$

Here ε is the eigenenergy of the state with quantum number n_x. The ω_x^2-term in (29) can be safely neglected, so $\overline{\varepsilon}(k_x) \approx \varepsilon(k_x)$. Hamiltonian (28) depends quadratically on x, therefore, having in mind the interchange $k_x \to x$, $x \to k_x$, it is easy to find the semiclassical eigenfunction of (28) in the momentum representation.

$$\Psi^2(k_x, \varepsilon) = \frac{1}{N(\varepsilon)\sqrt{\varepsilon - \overline{\varepsilon}(k_x)}} \tag{30}$$

The eigenenergy ε is determined by the Bohr-Sommerfeld quantization condition

$$4 \cdot \sqrt{\frac{2}{m\omega_x^2}} \int_0^{k_{max}} \sqrt{\varepsilon - \overline{\varepsilon}(k_x)} dk_x = 2\pi n_x \ , \tag{31}$$

where k_{max} is the turning point in the momentum space, $\overline{\varepsilon}(k_{max}) = \epsilon$. The normalization coefficient in Eq. (30) is

$$N(\varepsilon) = \int_0^{k_{max}} \frac{dk_x}{\sqrt{\varepsilon - \overline{\varepsilon}(k_x)}} \ . \tag{32}$$

This normalization assumes that the momentum in (30) is always positive, $k_x > 0$.

The Zeeman splitting of the oscillator level is given by usual perturbation theory with wave function (30) and with the B-term in Eq. 27 being the perturbation

$$g(\varepsilon) = \int_0^{k_{max}} \Psi^2(k_x, \varepsilon)[g_{zz}(k_x) + g_\alpha(k_x)]\, dk_x \tag{33}$$
$$g_\alpha(k_x) = 4m^2\omega_x^2\alpha(k_x)x^2(k_x) \ ,$$

where $x^2(k_x)$ is defined by Eq. (29). We know the function $g(\varepsilon)$ from the numerical diagonalization of 3D Luttinger Hamiltonian, see Eq. (26). Functions $\Psi(k_x, \varepsilon)$, $\alpha(k_x)$ and $x(k_x)$ have been already calculated. In the next paragraph we explain how to invert the integral equation (33) and to find the function $g_{zz}(k_x)$.

To solve the integral equation (33) we use a well known mathematical method developed in classical mechanics for the purpose to determine potential in terms of known period of motion[35]. Here we briefly describe the method. We can rewrite Eq. (33) as

$$f(\varepsilon) = \int_0^{k_{\max}} \frac{g_{zz}(k_x)\, dk_x}{\sqrt{\varepsilon - \overline{\varepsilon}(k_x)}} \ , \tag{34}$$

where

$$f(\varepsilon) = N(\varepsilon)\left(g(\varepsilon) - \int_0^{k_{max}} \Psi^2(k_x, \varepsilon) g_\alpha(k_x)\, dk_x\right) \tag{35}$$

is known function. Changing the integration variable we transform (34) to

$$f(\varepsilon) = \int_0^{\varepsilon} \frac{h(\overline{\varepsilon})\, d\overline{\varepsilon}}{\sqrt{\varepsilon - \overline{\varepsilon}}}, \tag{36}$$

where

$$h(\overline{\varepsilon}) = \frac{g_{zz}(k(\overline{\varepsilon}))}{v(\overline{\varepsilon})}, \tag{37}$$

$v(\overline{\varepsilon}) = \partial\overline{\varepsilon}(k)/\partial k$ is the velocity. Next we integrate Eq. (36) over ε with the kernel $1/\sqrt{\eta - \varepsilon}$, where η is an external energy variable.

$$\int_0^{\eta} \frac{f(\varepsilon)\, d\varepsilon}{\sqrt{\eta - \varepsilon}} = \int_0^{\eta}\int_0^{\varepsilon} \frac{h(\overline{\varepsilon})\, d\overline{\varepsilon} d\varepsilon}{\sqrt{\eta - \varepsilon}\sqrt{\varepsilon - \overline{\varepsilon}}} = \pi \int_0^{\eta} h(\varepsilon)\, d\varepsilon \ . \tag{38}$$

Finally, differentiating Eq. (38) over η, we find the function $g_{zz}(k)$:

$$g_{zz}(k) = \frac{v(\eta)}{2\pi\sqrt{\eta}} \int_0^1 [f(\eta y) + 2\eta y f'(\eta y)] \frac{dy}{\sqrt{1-y}} \ , \tag{39}$$

where η and k are related as $\eta = \overline{\varepsilon}(k)$.

Eq. (39) solves the inverse problem. So, having the result (26) of the numerical diagonalization of 3D Luttinger Hamiltonian and using Eq. (39) we find the out-of-plane g-factor. Plots of $g_{zz}(k)$ for parabolic and rectangular quantum wells in GaAs and InAs are presented in Fig. 8.

Typical experimental densities correspond to the in-plane momentum $k = 0.5 \div 1.5$. According to Fig. 8, this region contains two points where g_{zz} changes its sign and these points can be achieved experimentally. Absolute value $|g_{zz}| \approx 5$ at $k \approx 1$ is consistent with experimental data, Ref.[14]

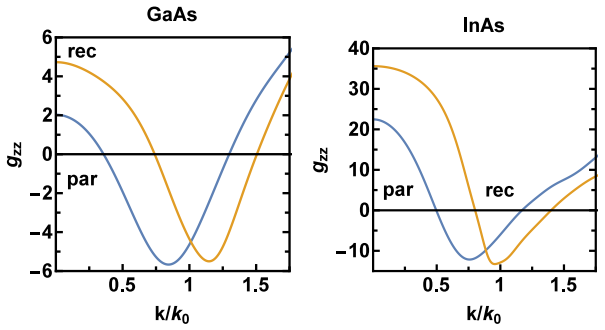

FIG. 8: Out-of-plane g-factor g_{zz} as function of the in-plane momentum. The g-factor is presented for parabolic and rectangular quantum wells in GaAs and InAs.

VII. CONCLUSIONS

We perform the 3D → 2D dimensional reduction of the Luttinger Hamiltonian for holes in zinc-blende semiconductors in the presence of a symmetric quantum well, a smooth lateral gate potential, and an uniform external magnetic field. Our results are applicable to all kinds of two-dimensional symmetric semiconductor heterostructures. The effective 2D Hamiltonian, Eq. (10), is written as a Ginzburg-Landau-type gradient expansion in gradients of the lateral potential. We develop general methods and techniques to calculate parameters of the effective Hamiltonian as functions of the hole momentum. We specifically present numerical results for the parabolic quantum well and for the infinite rectangular quantum well in GaAs and InAs. In the paper we obtain the following results. (i) We develop the method of calculation and calculate g-factors for the in-plane direction of the magnetic field. In particular, we point out that there are two kinematically different g-factors, g_1 and g_2. An important consequence of two different g-factors is anisotropic magnetic response in presence of anisotropic lateral gate potential. The g-factors as functions of the hole momentum are plotted in Fig. 4. (ii) We develop the method of calculation and calculate the spin-orbit interaction and the Darwin interaction related to the lateral gate potential. The functions α (spin-orbit) and β (Darwin) are plotted in Fig. 6 versus the hole momentum. (iii) We develop the method of calculation and calculate the g_{zz}-factor for the out-of-plane direction of the magnetic field. We also point out that in presence of a gate potential (quantum point contact or a quantum dot) magnetic response is not only due to g_{zz}, there is a part of the response related to the gate potential which is also calculated. The plot of g_{zz} versus momentum is presented in Fig. 8.

VIII. ACKNOWLEDGMENTS

We thank A. Hamilton and A. Srinivasan for useful discussions and interest to the work. We are also grateful to L. E. Golub and U. Züelicke for valuable communications. The work has been supported by the Australian Research Council grant DP160103630.

[1] G. Dresselhaus, *Phys. Rev.* **100**, 580 (1955).
[2] Yu. A. Bychkov and E. I. Rashba, Sov. Phys. - JETP Lett. **39**, 78 (1984).
[3] R. L. Kallaher, J. J. Heremans, N. Goel, S. J. Chung, and M. B. Santos, *Phys. Rev. B* **81**, 075303 (2010).
[4] J. P. Heida, B. J. van Wees, J. J. Kuipers, T. M. Klapwijk, and G. Borghs, *Phys. Rev. B* **57**, 11911 (1998).
[5] J. M. Luttinger, *Phys. Rev* **102**, 1030 (1956).
[6] M. Cardona, N. E. Christensen, and G. Fasol, *Phys. Rev. B* **38**, 1806 (1988).
[7] R. Winkler, *Spin-Orbit Coupling Effects in Two- Dimensional Electron and Hole Systems*, Springer-Verlag, Berlin, Heidelberg, 2003.
[8] T. Li, L. A. Yeoh, A. Srinivasan, O. Klochan, D. A. Ritchie, M. Y. Simmons, O. P. Sushkov, and A. R. Hamilton, *Phys. Rev. B* **93**, 205424 (2016).
[9] R. Danneau, O. Klochan, W. R. Clarke, L. H. Ho, A. P. Micolich, M. Y. Simmons, A. R. Hamilton, M. Pepper, D. A. Ritchie, and U. Züelicke, *Phys. Rev. Lett.* **97**, 026403 (2006).
[10] S. P. Koduvayur, L. P. Rokhinson, D. C. Tsui, L. N. Pfeiffer, and K. W. West, *Phys. Rev. Lett.* **100**, 126401 (2008).
[11] O. Klochan, A. P. Micolich, L. H. Ho, A. R. Hamilton, K. Muraki and Y. Hirayama, *New J. Phys.* **11**, 043018 (2009).
[12] J. C. H. Chen, O. Klochan, A. P. Micolich, A. R. Hamilton, T. P. Martin, L. H. Ho, U. Züelicke, D. Reuter and A. D. Wieck, *New J. Phys.* **12**, 033043 (2010).
[13] Y. Komijani, M. Csontos, I. Shorubalko, U. Züelicke, T. Ihn, K. Ensslin, D. Reuter and A. D. Wieck, *EPL* **102**, 3 (2013).
[14] A. Srinivasan, L. A. Yeoh, O. Klochan, T. P.Martin, J. C. H. Chen, A. P. Micolich, A. R. Hamilton, D. Reuter, and A. D. Wieck, *Nano Lett.* **2013**, 13(1).
[15] F. Nichele, S. Chesi, S. Hennel, A. Wittmann, C. Gerl, W. Wegscheider, D. Loss, T. Ihn, and K. Ensslin, *Phys. Rev. Lett.* **113**, 046801 (2014).
[16] V. A. Kulbachinskii, P. V. Gurin, O. V. Vikhrova, Yu. A. Danilov, B. N. Zvonkov, *JPCS* **100**, 042025 (2008).
[17] C. D. Cress, Ch. G. Bailey, S. M. Hubbard, D M. Wilf, S. G. Bailej, and R. P.Raffaelle, *PVSC* (2008).
[18] O. Klochan, A. P. Micolich, A. R. Hamilton, K. Trunov, D. Reuter, and A. D. Wieck, *Phys. Rev. Lett.* **107**, 076805 (2011).
[19] D. V. Bulaev and D. Loss, *Phys. Rev. Lett.* **98**, 097202 (2007).
[20] L. A. Yeoh, A. Srinivasan, O. Klochan, R. Winkler, U. Züelicke, M.Y. Simmons, D.A. Ritchie, M. Pepper, and A.R. Hamilton, *Phys. Rev. Lett.* **113**, 236401 (2014).
[21] E. Bangert and G. Landwehr, *Surf. Sci.* **170**, (1986).

[22] R. Winkler, M. Merkler, T. Darnhofer, and U. Rössler, *Phys. Rev. B* **53**, 10858 (1996).
[23] M. Failla, M. Myronov, C. Morrison, D. R. Leadley, and J. Lloyd-Hughes, *Phys. Rev. B* **92**, 045303 (2015).
[24] Th. Wimbauer, K. Oettinger, Al. L. Efros, B. K. Meyer, and H. Brugger, *Phys. Rev. B* **50**, 8889 (1994).
[25] M. V. Durnev, M. M. Glazov, E. L. Ivchenko, M. Jo, T. Mano, T. Kuroda, K. Sakoda, S. Kunz, G. Sallen, L. Bouet, X. Marie, D. Lagarde, T. Amand, and B. Urbaszek, *Phys. Rev. B* **87**, 085315 (2013).
[26] I. L. Drichko, V. A. Malysh, I. Yu. Smirnov, L. E. Golub, S. A. Tarasenko, A. V. Suslov, O. A. Mironov, M. Kummer, and H. von Känel, *Phys. Rev. B* **90**, 125436 (2014).
[27] G. E. Simion and Y. B. Lyanda-Geller, *Phys. Rev. B* **90**, 195410 (2014).
[28] C. Gradl, M. Kempf, D. Schuh, D. Bougeard, R. Winkler, C. Schüller, and T. Korn, *Phys. Rev. B* **90**, 165439 (2014).
[29] L. C. Andreani, A. Pasquarello, and F. Bassani, *Phys. Rev. B* **36**, 5887 (1987).
[30] O. P. Sushkov and A. H. Castro Neto, Phys. Rev. Lett., **110**, 186601 (2013).
[31] V. B. Berestetskii, E. M. Lifshitz, L. P. Pitaevskii, *Quantum Electrodynamics*, Butterworth-Heinemann, Science, 1982.
[32] A. Baldereschi and N. O. Lipari, *Phys. Rev. B* **8**, 2697 (1973).
[33] R. Winkler, S. J. Papadakis, E. P. De Poortere, and M. Shayegan, *Phys. Rev. Lett.* **85**, 4574 (2000).
[34] R. Winkler, D. Culcer, S. J. Papadakis, B. Habib and M. Shayegan, *Semicond. Sci. Technol.*, 23 (2008).
[35] L.D. Landau and E. M. Lifshitz Mechanics, sdection (Volume 1 of A Course of Theoretical Physics) Pergamon Press 1969.